# A microstructural investigation of gas atomized Raney type Al-27.5 at.% Ni catalyst precursor alloys

Mullis, A.M.; Bigg, T.D.; Adkins, Nicholas

*DOI:*
10.1016/j.jallcom.2015.05.142



*Document Version*
Peer reviewed version

*Citation for published version (Harvard):*
Mullis, AM, Bigg, TD & Adkins, N 2015, 'A microstructural investigation of gas atomized Raney type Al-27.5 at.% Ni catalyst precursor alloys', *Journal of Alloys and Compounds*, vol. 648, pp. 139-148. https://doi.org/10.1016/j.jallcom.2015.05.142

# Accepted Manuscript


A Microstructural Investigation of Gas Atomized Raney Type Al-27.5 at.%Ni Catalyst Precursor Alloys

A.M. Mullis, T.D. Bigg, N.J. Adkins

PII: S0925-8388(15)01447-4

DOI: 10.1016/j.jallcom.2015.05.142

Reference: JALCOM 34259

To appear in: *Journal of Alloys and Compounds*

Received Date: 18 November 2014

Revised Date: 17 March 2015

Accepted Date: 1 May 2015

Please cite this article as: A.M. Mullis, T.D. Bigg, N.J. Adkins, A Microstructural Investigation of Gas Atomized Raney Type Al-27.5 at.%Ni Catalyst Precursor Alloys, *Journal of Alloys and Compounds* (2015), doi: 10.1016/j.jallcom.2015.05.142.

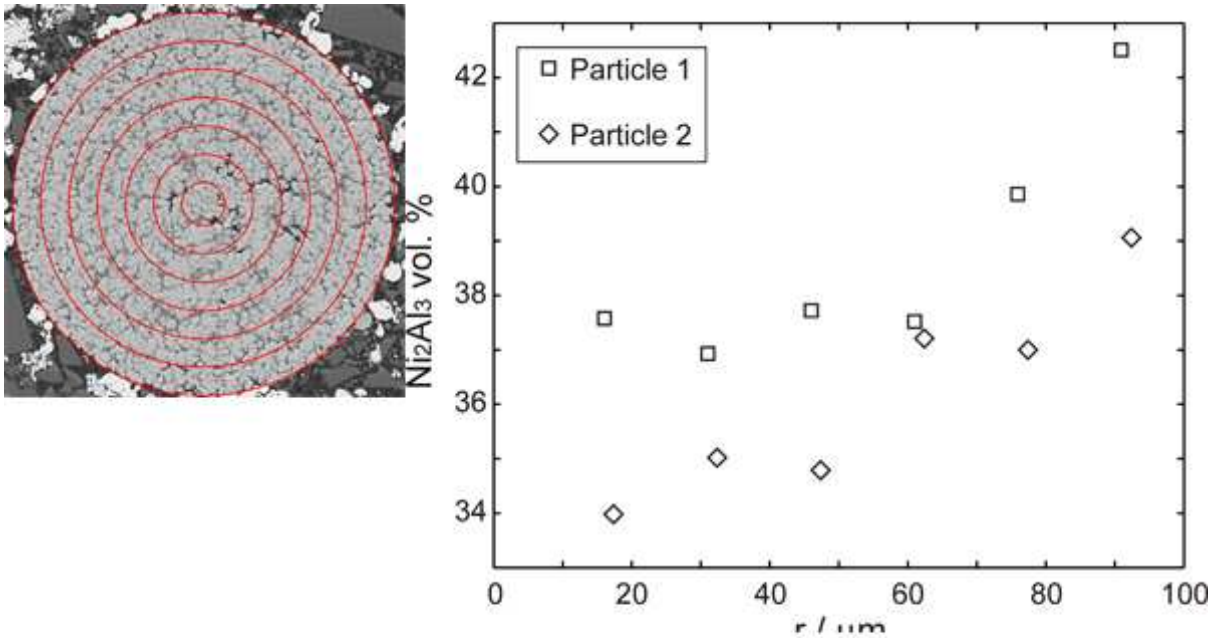


Microstructural examiation of annular sections of a Raney Ni catalyst particle showing significant variation in the amount of $Ni_2Al_3$ phase retained near the surface. This suggest more rapid cooling near the surface which would not normally be considered relevant for small (200 μm diameter) particles.

# A Microstructural Investigation of Gas Atomized Raney Type Al-27.5 at.%Ni Catalyst Precursor Alloys

*A.M. Mullis*[1a], *T.D. Bigg*[1b] and *N.J. Adkins*[2c]

[1]Institute for Materials Research, University of Leeds, Leeds LS2 9JT, UK.
[2]IRC in Materials Processing, University of Birmingham, Edgbaston, Birmingham B15-2TT.

a) a.m.mullis@leeds.ac.uk b) t.bigg@leeds.ac.uk c) n.j.e.adkins@bham.ac.uk

## *Abstract*

Quantitative image analysis has been used to investigate the phase composition of gas atomized powders of a Raney type Ni catalyst precursor alloys of composition Al-27.5 at.% Ni in the powder size range 150-212 μm. We find that there are considerable variations in phase composition both between powders from the same batch and as a function distance from the particle surface within individual particles. Such variations may have significant implications for the future production and uptake of such catalysts, including the necessity for post-production crushing of gas atomized powders. Models are proposed to account for both variations.

**Keywords**: Raney-type nickel catalysts; Nickel aluminium alloy; Gas atomisation process

## 1 Introduction

Skeletal, or sponge metal, catalysts have found wide application in a range of hydrogenation and dehydrogenation reactions [1], as well as in hydrogenolysis [2] and hydrolysis reactions [3]. Of these skeletal metal catalysts, Raney type Ni [4] is by far the most common. Traditionally Raney Ni catalysts are produced by casting ingots of a 50-50 wt.% mixture of Ni and Al (which due to the large density difference is Al-31.5 at.% Ni) that are subsequently crushed into coarse powders so that the catalyst can be activated by leaching in a concentrated solution of alkali metal hydroxide [5]. During this process much of the Al is removed from the precursor alloy to leave a nano-crystalline Ni structure, which is the active catalyst.

A number of studies [see e.g. 6] have shown that the main phases present in the precursor Ni-Al alloy are the intermetallics $Ni_2Al_3$ and $NiAl_3$, together with an Al-$NiAl_3$ eutectic. This is broadly in agreement with the binary phase diagram, wherein the first phase to form at the liquidus temperature of 1623 K for the Al-31.5 at.% Ni composition is NiAl. This subsequently transforms to $Ni_2Al_3$ via a peritectic reaction at 1406 K. As NiAl is not generally observed in Raney type Ni precursor alloys [7], it is generally assumed that this peritectic reaction goes to completion. Upon further cooling a second peritectic is encountered at 1127 K, wherein $Ni_2Al_3$ is converted to $NiAl_3$. The retention of significant fractions of $Ni_2Al_3$ in the as-solidified precursor alloys indicates that, unlike the L + NiAl $\rightarrow$ $Ni_2Al_3$ reaction, this peritectic is not

easily able to go to completion. Solidification ends at 912 K with the formation of an Al-$NiAl_3$ eutectic. The Al-rich end of the Al-Ni phase diagram is shown in **Figure 1**.

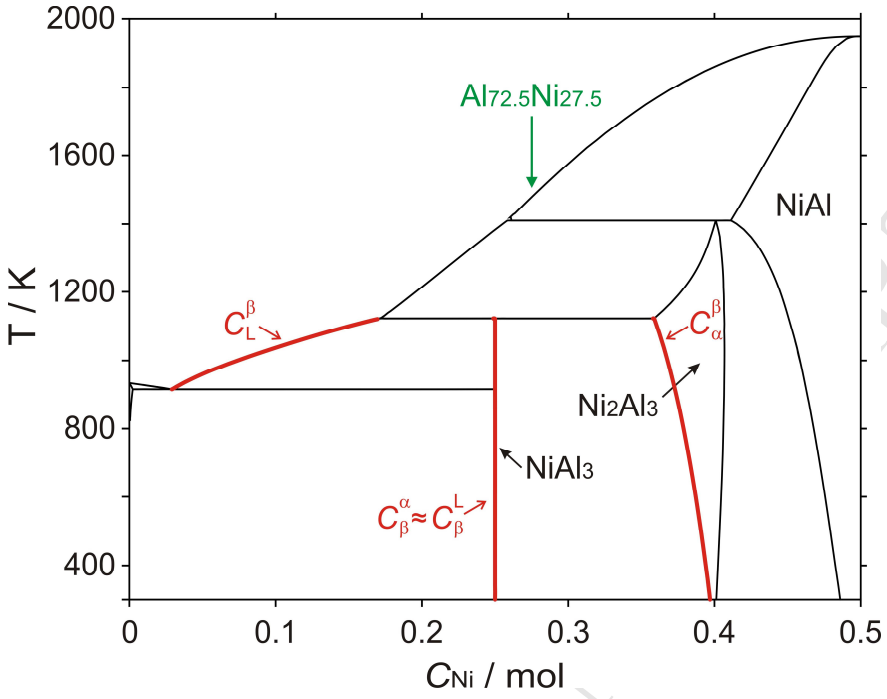


**Figure 1** –Al-rich portion of the Al-Ni phase diagram showing the main phases present in Raney type Ni catalyst precursor alloys ($Ni_2Al_3$, $NiAl_3$ and Al-$NiAl_3$ eutectic), together with the 27.5 at.% starting composition of the liquid which forms the basis for this study. $C_\beta^\alpha$ etc. refer to the terms in Equ. (1), which describes the rate at which the solid-solid peritectic transformation occurs, in this case with reference to the $Ni_2Al_3 + L \rightarrow NiAl_3$ peritectic (see below).

Each of the equilibrium phases, $Ni_2Al_3$, $NiAl_3$ and Al, responds differently to leaching. $NiAl_3$ leaches easily and gives the most active catalyst [6, 8] but is easily friable, meaning that in its pure form it is unsuitable for applications such as slurry and tubular bed reactors [9]. $Ni_2Al_3$ is less easily leached than $NiAl_3$, and is therefore less catalytically active, but retains greater structural integrity [6, 8]. For this reason it is also considered an important constituent of most Raney type catalyst precursor alloys [10], with the original dendritic structure of the $Ni_2Al_3$ remaining after leaching to support the active nano-crystalline Ni phase produced by the leaching of $NiAl_3$. The Al-$NiAl_3$ eutectic, being largely Al by volume, is almost entirely lost during leaching, producing a microporous network of channels by which both the leaching agent can enter the precursor particles, and subsequently by which the chemical reagents can enter the activated catalyst. Consequently, anything that changes the balance of phases within the catalyst, be that the composition of the precursor alloy or its cooling rate during solidification, can significantly alter the performance of the final, activated catalyst.

A number of attempts have been made to improve the performance of Raney type Ni catalysts by employing novel processing routes, in particular rapid solidification processing of the precursor alloy. A number of studies have shown that melt spun

ribbons [11, 12] could lead to a catalyst with higher activity and could allow the possibility of higher Al concentrations, something that proves difficult via the cast-crush route due to the extreme friability of the resulting catalyst [10]. In recent years there has been an upsurge in interest in gas atomized Raney type Ni precursors [13-15], with Al concentrations in the range 68.5-82.5 at.% being investigated. Gas atomization would be expected to give cooling rates of the order $10^2$-$10^5$ K $s^{-1}$ [16-18] (depending upon particle size and, to a lesser extent, gas type) with catalytic activities in the subsequently activated catalyst [14] more than twice that of conventional Raney type Ni being reported. Generally, the best catalytic performance has been found for relatively large particles that would have experienced cooling rates towards the lower end of the spectrum quoted above. There is some evidence that subsequent crushing of the atomized precursor alloy to produce an ultra-fine powder, that nevertheless experienced a low-intermediate cooling rate, gives the optimum catalytic performance.

However, our lack of understanding of this system may in part arise as the kinetics of peritectic reactions have been much less well studied than most other solidification morphologies. Kerr & Kurz [19] describe peritectic solidification as comprising three stages. For the transformation $\alpha + L \rightarrow \beta$ these are:

i) Liquid-solid peritectic reaction (PR): The initiating stage of the transformation in which a thin shell of β overgrows the primary α phase. Growth occurs at the triple junction at which all three phases remain in contact. This stage terminates when the α phase is completely encased in a thin layer of β. It is important in terms of the nucleation of β, but is unlikely to contribute significantly to either the increase in volume of β or the corresponding decrease in volume of α.
ii) Solid-solid peritectic transformation (SSPT): Once the α phase is completely encased in β any further transformation of α to β requires diffusion through the solid β layer. This is likely to make such transformations sluggish. It is normally taken that the thickness, Δ, of the β layer is given by [20]

$$\frac{\Delta^2}{2\tau} = D_\beta \frac{\left(C_\beta^{\mathrm{L}} - C_\beta^\alpha\right)\left(C_{\mathrm{L}}^\beta - C_\alpha^\beta\right)}{\left(C_{\mathrm{L}}^\beta - C_\beta\right)\left(C_\beta - C_\alpha^\beta\right)} \qquad (1)$$

where $D_\beta$ is the average interdiffusion coefficient in the β phase, $C_\beta^\alpha$ and $C_\alpha^\beta$ are the compositions of the β phase in equilibrium with the α phase (or liquid in the case of $C_\beta^{\mathrm{L}}$ and $C_{\mathrm{L}}^\beta$), and vice-versa, $C_\beta$ is the average composition of the β phase and $\tau$ is the time available at, or below, the peritectic temperature, before the onset of significant direct solidification (DS) of β (see iii below). With reference to the Al-Ni phase diagram we note that the $Ni_2Al_3$ (α) + L → $NiAl_3$ (β) peritectic reaction is Type C in the classification described in [20, 21], i.e. $NiAl_3$ is a line compound so that $C_\beta^{\mathrm{L}} \approx C_\beta^\alpha$, wherein the transformation rate is expected to be slow. The values of $C_\beta^\alpha$, $C_\alpha^\beta$, $C_\beta^{\mathrm{L}}$ and $C_{\mathrm{L}}^\beta$ are given in **Figure 1** for the $Ni_2Al_3$ + L → $NiAl_3$ peritectic.

iii) Direct solidification of peritectic phase (DS): As the temperature drops below that of the peritectic, $T_p$, the driving force for the direct solidification of β from the liquid will increase more rapidly than for the solid-solid transformation of α to β. This leads to the direct growth of β from the liquid. In many situations this will be the major contributor to the volume of β found in the as-solidified sample, but will of course not reduce the volume of α as is the case for the PR and SSPT stages.

A number of papers have shown that the phase evolution in Raney type Ni precursor alloys as a function of cooling rate may be complex. Neutron and X-ray diffraction studies [13, 21] have shown that for Ni concentrations of ≥ 25 at.% the fraction of $NiAl_3$ decreases with increasing cooling rates (which for gas atomization corresponds to decreasing particle diameter) while the fraction of $Ni_2Al_3$ increases. This can be understood in terms of the kinetics of the SSPT stage of the peritectic reaction $Ni_2Al_3 + L \rightarrow NiAl_3$, as defined above, this being the stage in the peritectic that is responsible for the majority of the conversion of $Ni_2Al_3$. Due to the reliance upon solid-state diffusion this is a relatively slow conversion, wherein high cooling rates restrict the time available for this reaction to proceed, giving more retained $Ni_2Al_3$ (and hence less $NiAl_3$) in the as-solidified microstructure. Conversely, for Ni concentrations of < 25 at.% the fraction of $NiAl_3$ increases with increasing cooling rates. The most likely explanation for this is that the stability field for the primary solidification to $Ni_2Al_3$ becomes quite restricted at low Ni concentrations, such that some droplets attain sufficient undercooling to bypass the formation of $Ni_2Al_3$, solidifying instead to give $NiAl_3$ as the primary solidification phase.

A further complexity when considering gas atomized powders is that the stochastic nature of the nucleation process within a population of rapidly cooling droplets leads to considerable variability within a sample of notionally similar droplets. To a good first approximation, droplets of the same size will be subjected to the same cooling rate. However, it is not true that all droplets of the same size will solidify at the same undercooling, as this is controlled by nucleation which is a stochastic process. Solidification of the liquid might be catalysed by a potent nucleation site, such as an oxide, and in such cases deep undercooling would not be expected. However, the catalytic effect of active nuclei can be restricted by dispersing the liquid into a large number of small droplets that solidify individually. This is often referred to as melt sub-division. In this stochastic process, a range of undercoolings from low to relatively high would be expected in each size range due to the variation in nuclei density and potency. Consequently, techniques such as neutron and X-ray diffraction, which provide a bulk average for the material, can hide considerable natural variability within the particle population.

Recent studies have shown that during rapid solidification of the melt additional metastable phases may form, including $Ni_2Al_9$ and a decagonal quasicrystalline phase [22]. The composition of the decagonal phase has been determined to be between 24 and 30 at% Ni and it shows distinct structural similarities to $Ni_2Al_3$ [22]. However, *in situ* synchrotron studies on levitated droplets have shown that the formation of this phase requires the $Ni_2Al_3$ + L mush to be undercooled ≥155 K below the $NiAl_3$ peritectic temperature without the nucleation of the $NiAl_3$ phase [23, 24]. Both phases have been shown to be retained during splat quenching [22] and the decagonal phase during gas atomization, if the particle diameter is < 38 μm [25]. Upon nucleation of

$NiAl_3$ the decagonal phase is converted rapidly to $NiAl_3$ [23]. Given that $NiAl_3$ is a stoichiometric intermetallic, little evidence for the origin of the $NiAl_3$ is likely to be retained in the as-solidified sample and consequently we may conjecture this is likely to have little effect on the catalytic properties of gas atomized Raney powders.

In this paper we explore a technique for analysing the kinetics of the $Ni_2Al_3 + L \rightarrow NiAl_3$ peritectic transformation using a method based on the image analysis of annular sections of gas atomized Al-27.5 at.% Ni powders in the diameter range 150-212 μm. Despite the small size of these powders the surface will be subject to more rapid cooling than the interior, leading to small, but quantifiable, radial variations in the phase composition of the particles. The technique, being based on the examination of individual particles, also yields information on the natural variability within the particle distribution. Interpretation of the results is aided by numerical modelling of heat transfer within the cooling droplets.

## 2 Experimental Method and Analysis Techniques

### 2.1 Powder Preparation

Powders of the Raney precursor alloy were prepared by close-coupled gas atomization. The atomizer utilises a simple die of the discrete jet type with 18 cylindrical jets of 0.5 mm diameter arranged around a tapered melt delivery nozzle at an apex angle of 45°. The design is similar to the USAG [26] and Ames HPGA-I [27] designs. The liquid metal is delivered to the tip of the atomization nozzle via a central 2 mm diameter bore in the nozzle. In order to ensure the smooth flow of liquid metal an over pressure of 40 kPa is applied to the reservoir above the atomization nozzle. In order to prevent oxidation of the liquid metal Ar was used as the atomizing gas. The atomization pressure was 3.5 MPa, giving a gas flow rate of 0.049 kg $s^{-1}$. A melt pour temperature of 200 K above the liquidus was used to ensure smooth flow of the melt.

The alloy selected for this investigation was Al-27.5 at.% Ni, the reasons being:

1) this composition yields approximately equal volume fractions of the $Ni_2Al_3$ and $NiAl_3$ phases, which reduces the errors associated with the measurement technique,
2) The liquidus temperature for this composition is 1480 K wherein it is unlikely that sufficient undercooling could be achieved in any droplet to bypass the $L + Ni_2Al_3 \rightarrow NiAl_3$ peritectic (1127 K), as might be the case for some of the more Al-rich alloys.

Gas atomization typically produces a broad range of particles sizes, with the process used here typically producing powders in the 20-250 μm range. As the cooling rate of particles varies with particle size, a sieving procedure was employed in order to classify the particles with respect to this important processing parameter. Particles in the 150-212 μm size range were selected for further analysis as these particles, which are towards the upper end of the size range produced, have the potential to show the largest difference in cooling rate between the surface and centre of the particles and because their larger size permits better counting statistics when analysing the variation within individual droplets. It is also crushed variants of these relatively large particles that have been shown to give the highest catalytic activity.

The average cooling rate for particles produced using the same atomization configuration as utilised here has been measured by [18] using the secondary dendrite arm spacing in Al-4 wt.% Cu alloys. They found that the cooling rate for particles in this size range to be of the order of 300 K $s^{-1}$, this low value being attributed largely to the high temperature of the circulating gas in the atomization chamber. Using the model of Libera et al. [28] the maximum undercooling prior to nucleation for this cooling rate can be estimated, wherein correspondingly low values of the undercooling (< 60 K) are obtained. Although the primary dendrite growth velocity has not been determined as a function of undercooling for this alloy, such determinations have been made [29] for both Al-25 at.% Ni and Al-30 at.% Ni, with growth velocities for these low undercoolings being ≈ 0.3 m $s^{-1}$ and 0.45 m $s^{-1}$ respectively.

## 2.2 Phase Composition & Solidification Morphology

In order to confirm that the powder sample contained only the expected $Ni_2Al_3$, $NiAl_3$ and α-Al phases, phase identification by powder XRD was employed prior to preparing polished sections for microstructural analysis. The powder was mounted using a low-background silicon single crystal substrate then measured using a Philips Xpert diffractometer fitted with a copper X-Ray tube. A nickel foil in the diffracted beam path was employed to filter the incoming X-Rays such that only Kα1 and Kα2 wavelengths were recorded by the detector. Diffraction data was collected over a 2-theta range of 10-80 degrees. To improve the statistics at high 2-theta angles the programmable divergence slit feature of the diffractometer was made use of. Post processing of the XRD measurements was initially performed using PANalytical software in order to apply a fixed divergence slit correction to the programmable divergence slit data. Crystallographic data for the phases present was obtained from the ICSD database. The resulting XRD trace is shown in **Figure 2**. The observed diffraction pattern can clearly be fitted by assuming only the three phases $Ni_2Al_3$, $NiAl_3$ and α-Al are present and this is assumed in the subsequent analysis of all SEM micrographs. Unlike [25], we find no evidence of any additional metastable phases in the gas atomized powders studied here. This is consistent with the relatively low cooling rates and consequently undercoolings experienced by these samples. In particular, the decagonal phase has only been observed to be retained in gas atomized droplets if the diameter is < 38 μm, wherein [18] estimates the cooling rate to be of the order of $10^4$ K $s^{-1}$, compared to 300 K $s^{-1}$ for the size of droplets considered here.

For microstructural analysis particles were hot mounted in conductive, copper-filled, Bakelite resin then ground and polished to a 1 μm finish using silicon carbide paper and diamond paste respectively. The mounted and prepared samples were then examined using a Carl Zeiss EVO MA15 electron microscope in backscatter detection mode. High resolution (2048x1536) greyscale images were obtained of individual particles. The images were collected in an 8 bit format, giving a density range of 0 to 255, with the minimum and maximum representing black and white respectively.

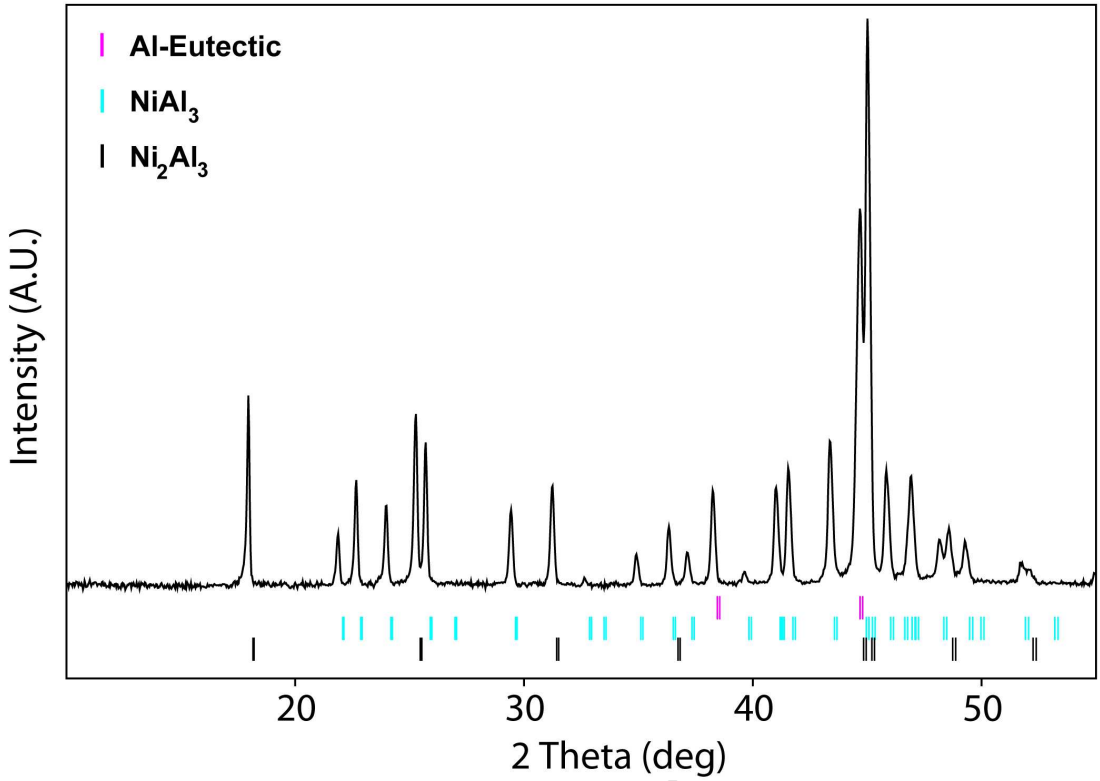


**Figure 2** – XRD trace for the Al-27.5 at.% Ni alloy studied here, showing the presence of $Ni_2Al_3$, $NiAl_3$ and α-Al only.

As the response from the backscatter detector varies according to atomic mass, and there exists a significant difference between the atomic mass of aluminium and nickel, the location of different phases in the particle can readily be resolved via density variation in the greyscale image. The nickel-rich $Ni_2Al_3$ phase scatters electrons most strongly, and so appears lightest, while the aluminium-eutectic phase scatters electrons least strongly, and therefore appears darkest. The $NiAl_3$ phase appears as a middling density, part way between that of the nickel-rich and aluminium-rich phases. Some much darker areas are also apparent, and inspection in normal secondary electron detector mode has revealed that these are slightly pitted areas, where small amounts of material have pulled out of the particle during the grinding and polishing process. Observing the way these pitted areas fit into the surrounding microstructure, it is considered most likely that these were areas of aluminium eutectic, and so it is appropriate to include these darker areas in the analysis as part of the aluminium rich phase. **Figure 3** shows a typical particle and the variations in image density that occur due to different phases present.

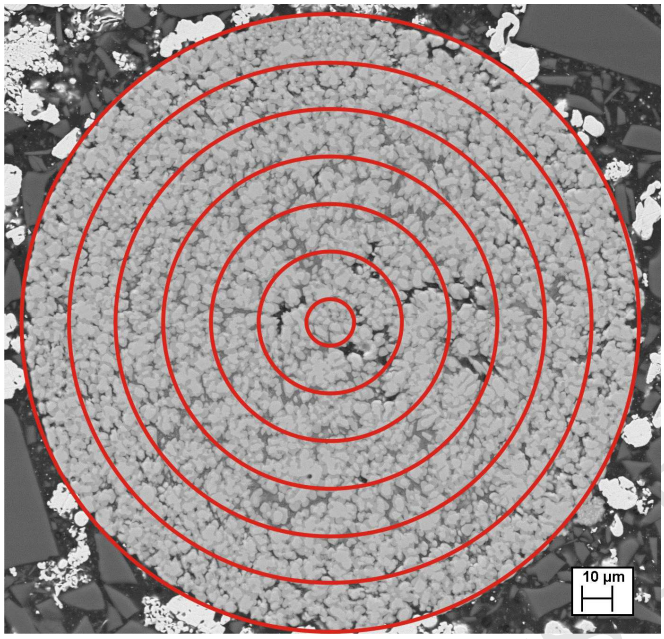


**Figure 3** – Electron backscatter image of a particle showing density variations due to different phases. Contrast outside the particle circumference is due to electrically conductive mounting compound. Also shown are the positions of the annuli used in the quantitative analysis discussed in Section 2.3.

**Figure 4a** shows a magnified region of a typical particle from the 212 – 150 µm sieve fraction. For clarity the $Ni_2Al_3$, which is the primary solidification phase, has been coloured red. The micrograph reveals numerous small dendritic fragments which suggests that the droplet has experienced multiple nucleation events. In contrast, **Figure 4b** shows an example of a powder from the 75-53 µm diameter sieve fraction where a single dendrite extends over much of the droplet, suggesting that the droplet consists of only one, or a a small number of, crystal(s). Even in the smaller size fractions such droplets are rare although there prevalence increases with decreasing particle size, presumably due to the rapid increase in cooling rate with decreasing particle size. Although these events are rare, **Figure 4b** illustrates that it is relatively straightforward to identify droplets that consist of only 1-2 crystallites from those that are highly polycrystalline.

The cause of such multiple nucleation structures is likely to be the violent nature of the atomization process. During the high pressure gas atomization process the melt stream is initially disrupted into relatively large droplets in the primary atomisation zone close to the melt delivery nozzle. It then undergoes further multiple break-up events into progressively smaller droplets in the secondary atomisation zone, with secondary atomization being the mechanism that plays the determining role in the final particle size. For a fluid that is being continuously cooled in flight during the atomization process it is therefore easy to conceive how the entrainment of surface oxides and small dendritic solidification fragments during repeated disruption of a droplet will result in the inclusion of copious nuclei within the droplet. It is these that lead to the refined, multiply nucleated, microstructure observed. The significance for this study is that the microstructure of the as-solidified 212 – 150 µm droplets considered here is refined, homogeneous and isotropic and as a consequence we can reasonably assume that the results obtained by sectioning the sample will be

independent of the sectioning angle and position. All droplets considered for quantitative analysis were highly polycrystalline.

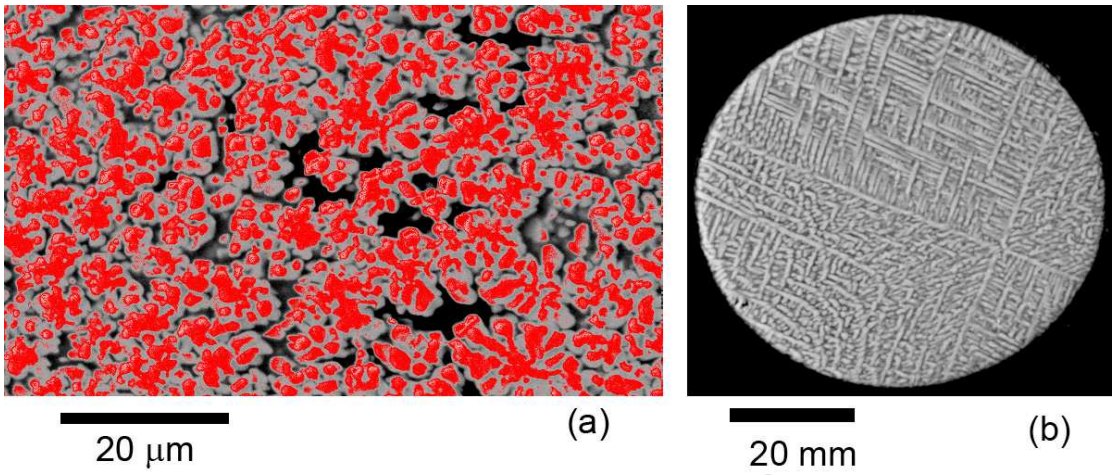


**Figure 4** – **(a)** Electron backscatter image of part of a particle from the 212-150 μm sieve fraction with the $Ni_2Al_3$ phase coloured red, wherein the highly fragmented nature of the primary solidification morphology is evident. Contrast this with **(b)** a relatively rare example of a droplet comprising only 1-2 crystallites from the 75-53 μm sieve fraction. Such droplets containing only 1-2 crystallites are easily identified in backscatter images and were not present in the larger size sieve fractions.

### 2.3 Quantitative Image Analysis

A histogram showing the grey-scale density distribution present in the particle shown in **Figure 3** (excluding the surrounding mount material) is shown in **Figure 5**, from which it can be seen that the analysis does indeed identify three distinct phases. The low plateau region at the left represents the aluminium eutectic phase, while the double peaks on the right represent the $NiAl_3$ and $Ni_2Al_3$ phases respectively. To ensure that individual particles being observed had been sectioned through, or close to their centre, when capturing images particles with an apparent diameter < 120 μm were excluded from the analysis (in this sample no particle has an actual diameter < 150 μm).

A combination of manual and automated analysis was used within the ImageJ [30] software package to extract information on the location of the different phases within the particle. The manual analysis consisted of initial inspection of each particle image in order to calculate the dimensions of the particle from the image scaling factor, and to determine the dimensions and position of an ellipse that fits the periphery of the particle. The contour plotting plugin for ImageJ was used on a zoomed portion of the particle image, in conjunction with the greyscale density distribution plot, to establish density ranges for each of the three phases. **Figure 6** shows the use of the ImageJ contour plotting plugin for a portion of **Figure 3**, with the contour thresholds set to greyscale values of 145 and 179. In this image, areas enclosed by blue lines have been designated as $Ni_2Al_3$ phase, areas enclosed by red lines are considered to be aluminium-eutectic, with the remaining area between red and blue lines being the intermediate $NiAl_3$ phase. The minimum image resolution used in this type of analysis was 5.92 pixels per μm, the highest resolution was 8.92 pixels per μm.

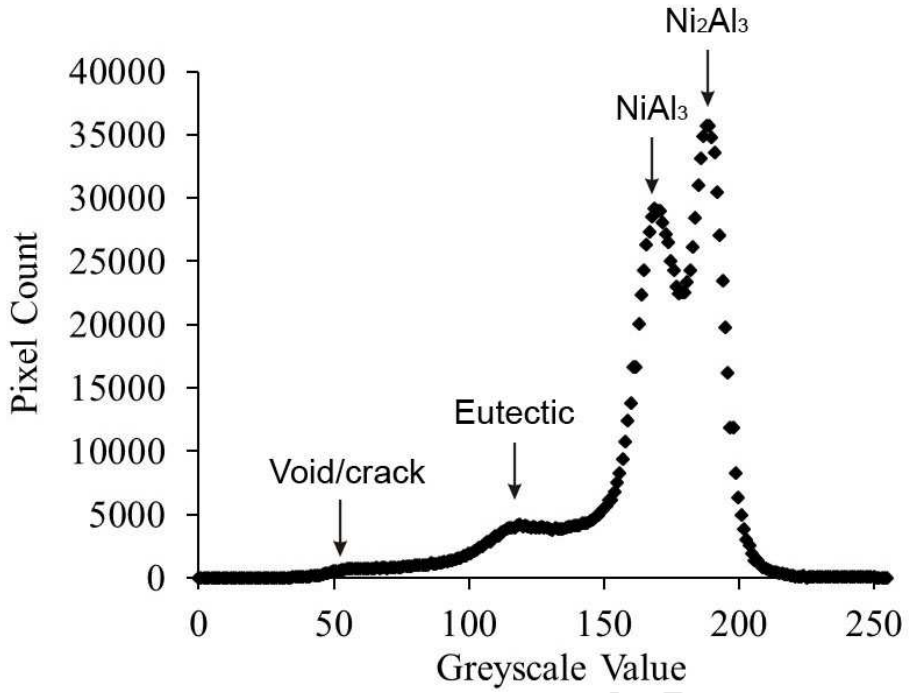


**Figure 5** – Grey scale density distribution for the particle shown in **Figure 3**.

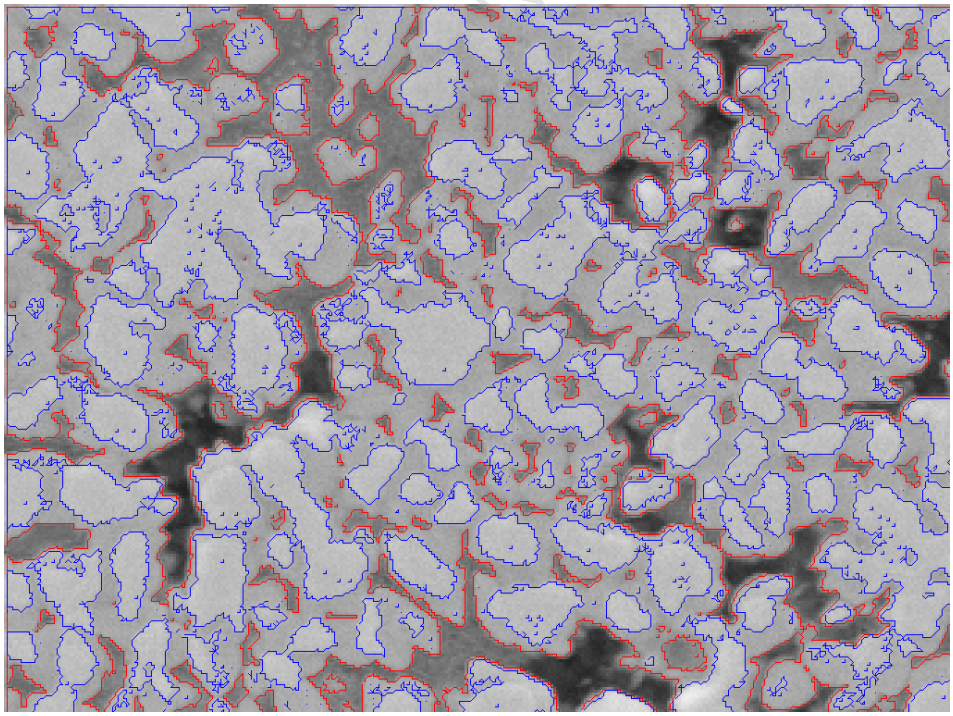

**Figure 6** – A zoomed-in portion of **Figure 3** showing the use of the ImageJ contour plotting add-on to establish density ranges for each phase.

Having acquired the dimensional, positional and image density parameters of the particle to be analysed, a macro program was written within ImageJ to extract image

density data from a series of ellipses of decreasing size. Within the macro, density data for each ellipse was subtracted from the preceding ellipse in order to produce density data for a series of annuli. The width of each annulus was 15 µm, with the procedure of reducing the ellipse axes 30 µm at a time being repeated until the centre of the particle was reached. This would typically result in six annular regions per particle (see **Figure** *3*), although a lesser number resulted for particles with the smallest apparent diameter. The macro then converted the annular greyscale data to a tabular output consisting of annulus mid-point diameter versus phase fraction for each particle. A total of 34 different particles were analysed by this method. The distribution of the apparent diameters of the particles surveyed, as they appear in cross-section, is as shown in **Figure 7**.

To cross check the reproducibility of the method four particles were selected at random and their phase composition independently re-examined and compared to the original determination. It was found that the mean (RMS) variation in the volume phase fraction of $Ni_2Al_3$, which is the main phase we will subsequently focus on, was 0.38% (0.73%), with the largest individual difference being 1.25%. As an approximate guide we would estimate the accuracy of the technique as around ± 0.5 at.%. As this is much smaller than the variation between different particles reported below we judge that the method is an appropriate means to determine the phase composition of gas atomized particles.

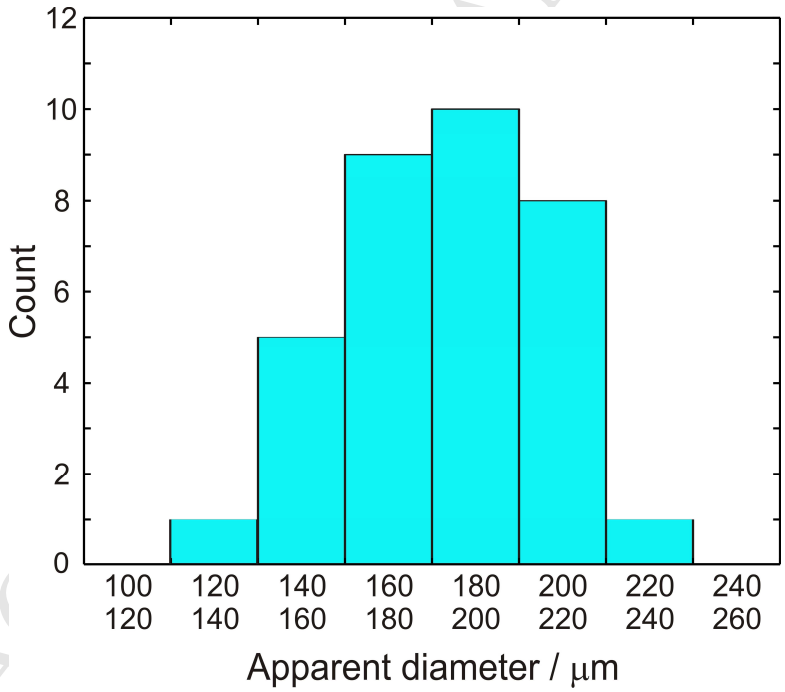


**Figure 7** – Apparent size distribution of the particles surveyed during the course of the investigation (upper and lower limit if size range in µm).

## 3 Results

The volume fraction of the three phases present, as a function of the radial distance from the centre of the particle, *r*, is shown for two typical particles in **Figure 8**. The following observations may be made regarding the radial phase variation across the population of droplets investigated here:

1) There is a considerable variation in the phase composition of the particles as a function of *r*.
2) This variation within particles does not appear to be random, nor is it in all cases well described by a linear relationship in *r*. Indeed, in many cases the trend appears to be for there to be a sharp rise in the amount of $Ni_2Al_3$ retained near the surface of the particle, with an approximately constant amount of $Ni_2Al_3$ near the centre of the particle. The amount of $NiAl_3$ appears in many cases to show the opposite trend, with less of this phase being present at the surface of the particle. This is apparent in the three points nearest the surface for the two particles shown.
3) No clear trend is observed in relation to the volume fraction of Al-eutectic.
4) Notwithstanding the observed phase variation within particles, there is an at least comparable variation in the mean level of the phases present between particles.

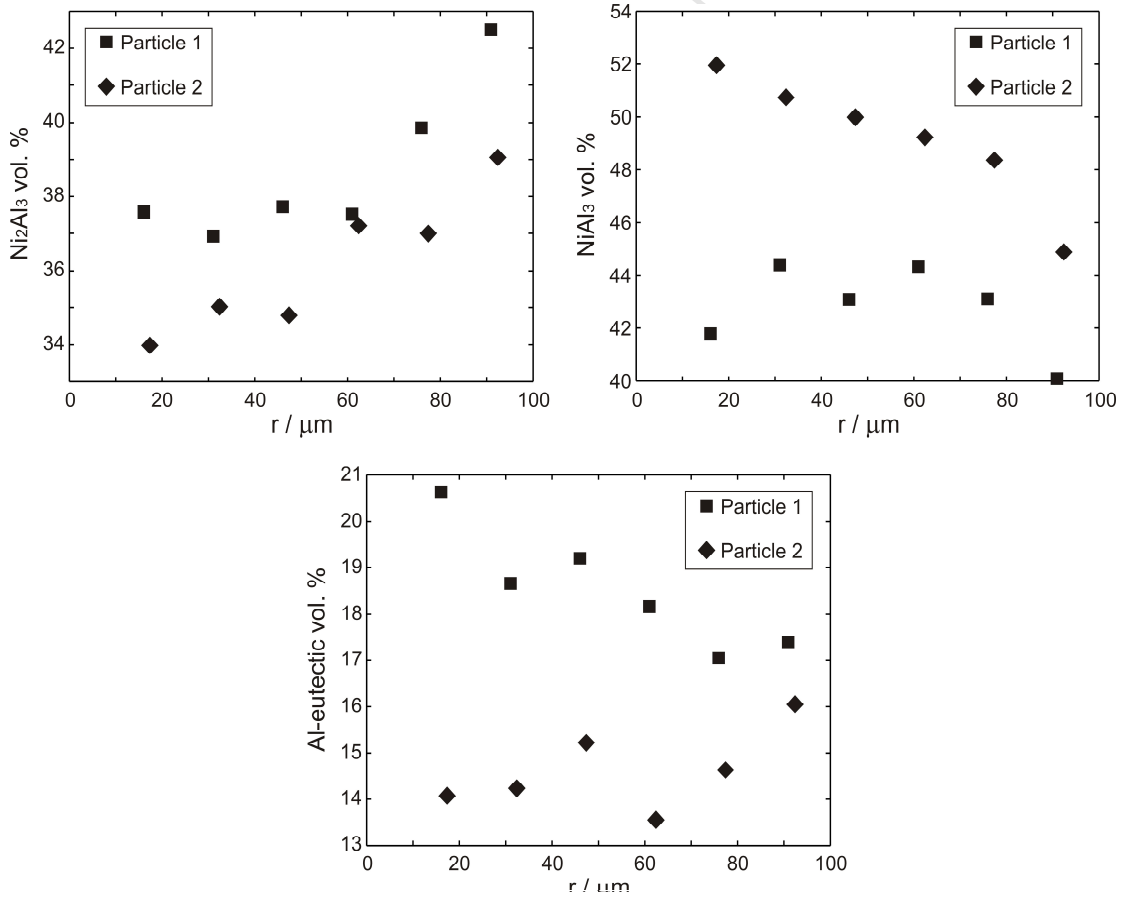


**Figure 8** – Phase composition as a function of radial co-ordinate *r* for two typical particles analysed.

The variability in the phase composition between the particles studied here is depicted in **Figure 9a-c**, in which we plot histograms of the mean volume fraction per particle for the three phases present. The mean and 2 sigma limits are 38.1 ± 5.5, 45.9 ± 6.2 and 16.1 ± 3.3 volume % for $Ni_2Al_3$, $NiAl_3$ and Al-eutectic respectively, with these limits being indicative of the level of natural variability we observe between particles from the same batch of powders. Although the phase composition of gas atomized Raney-Ni precursors has been extensively studied by both X-ray and neutron diffraction [13, 21] the large degree of variability observed between particles will not have been evident from such studies, although the variability within particles has been alluded to. In [21] a comparative analysis of gas atomized Raney-Ni precursors by neutron and X-ray diffraction is presented. With respect to the differences between the neutron and X-ray data sets and noting that neutrons will penetrate the whole particle but that X-rays are limited to a penetration depth of < 5 μm the authors conclude that 'the surface layer in a grain on the average contains relatively more of the $Al_3Ni_2$ phase than the bulk', which is consistent with the findings presented here. With respect to **Figure 9a** we also note that the distribution appears to be bimodal, a point to which we will return subsequently.

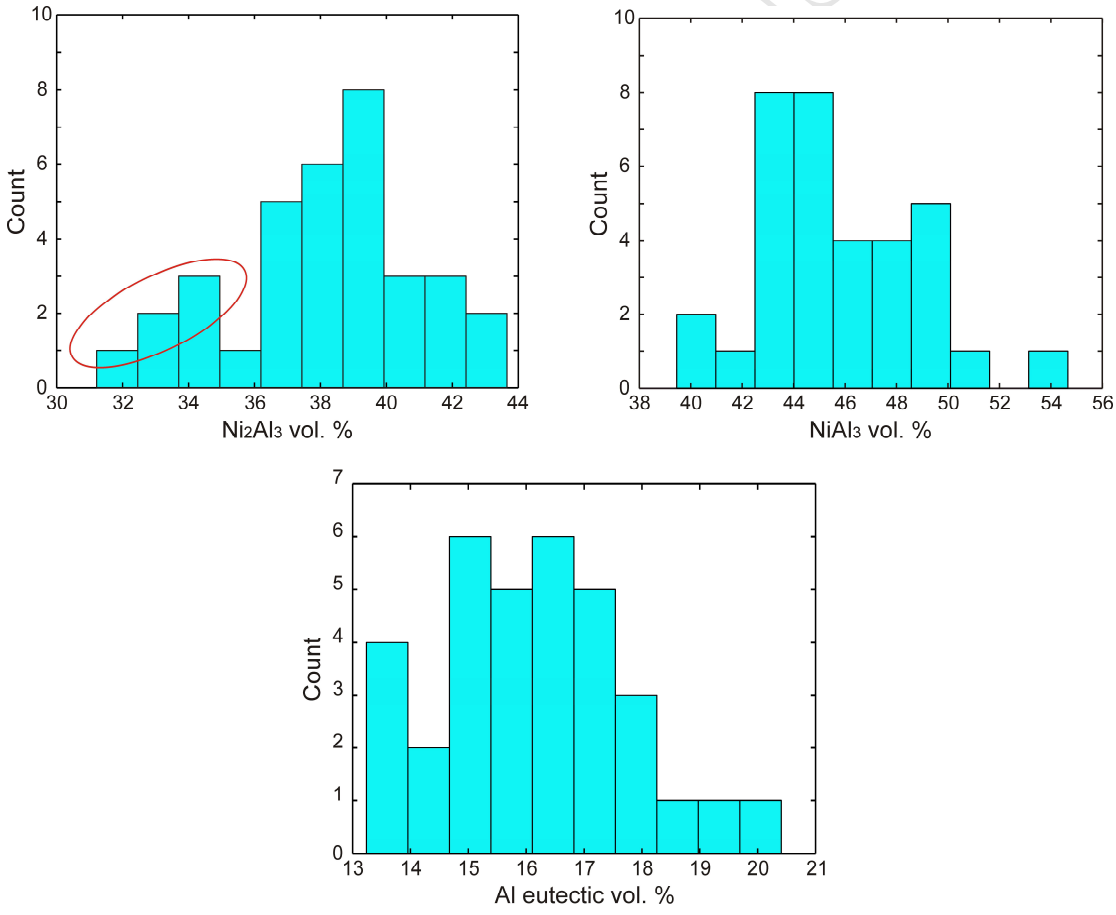


**Figure 9** – Average phase composition for the particles investigated in this study. The possibly bimodal distribution for $Ni_2Al_3$ content is highlighted.

The radial variation in the phase composition within particles has been characterised with reference to the $Ni_2Al_3$ phase only, this being the most reliable indicator of the SSPT stage of peritectic solidification. In this regard we are assuming that an initially

uniform network of dendritic fragments of $Ni_2Al_3$ were formed throughout the sample, either by direct solidification from the liquid or via the NiAl + L → $Ni_2Al_3$ peritectic going to completion. During the subsequent $Ni_2Al_3$ + L → $NiAl_3$ peritectic some of this $Ni_2Al_3$ will be converted to $NiAl_3$, wherein a reduction in the amount of $Ni_2Al_3$ observed will be recorded. Due to the large variability in the phase composition between particles the variation within particles has been characterised by determining the difference in $Ni_2Al_3$ composition between the inner and outer annuli of each particle, rather than by the absolute amount of the phase present. A histogram of these results is given as **Figure 10**, in which a positive difference indicates more $Ni_2Al_3$ being retained in the outer annulus.

As with the phase composition between particles, very significant variability within particles is observed. The variation range is -5.0 to +9.5 vol.%, with the mean, RMS and 2 sigma limits being 2.8, 4.8 and ± 4.0 vol. % respectively. Given the small size of the droplets the extent of the radial variation within droplets is quite surprising, although it is consistent with the findings of [21], wherein differences between the $Ni_2Al_3$ phase fraction as determined by neutron and X-ray diffraction on 150-212 μm powders of the order of 10 wt.% were observed. Equally surprising is the fact that a small number of droplets show a negative variation, i.e. that more $Ni_2Al_3$ is retained in the centre of the droplet than at its surface. This is the opposite of what would be expected for a droplet which is cooling more rapidly at its surface than in the centre, as more time should be available in the droplet centre for the peritectic to proceed. However, when we look at the individual particles which display a large negative variation, these all come from the region circled in **Figure 9a**, i.e. those particles that already display an anomalously low fraction of $Ni_2Al_3$ and which give rise to the apparently bimodal nature of the distribution shown in **Figure 9a**.

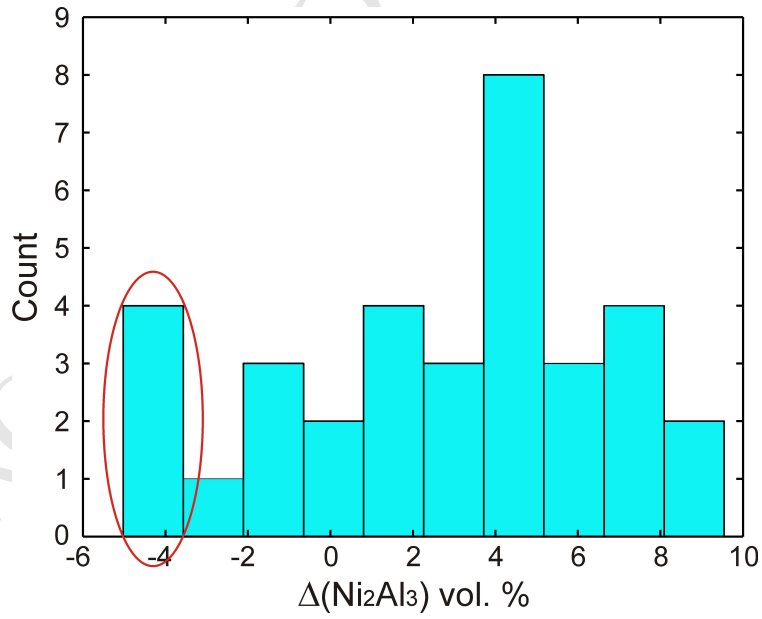


**Figure 10** – Difference in $Ni_2Al_3$ content between the centre and outer most annulus for the particles investigated in this study (positive difference indicates more $Ni_2Al_3$ retained in the outer most annulus of the particle). The particles circled are the same group as circled in **Figure 9a**.

## 4 Discussion

In terms of the solidification pathway for this alloy we can account for the majority of these observations as follows. During the gas atomization process the melt stream will be repeatedly disrupted so as to form a spray of fine molten droplets which will proceed to cool rapidly. At some point below the liquidus temperature nucleation will occur, resulting in the primary solidification of $Ni_2Al_3$. As seems likely from the microstructure of these larger droplets, the violence of the atomization process will result in fragmentation of these primary dendrites and possibly of the whole droplet as it passes through the secondary atomization zone. For very low undercoolings we may see the growth of NiAl with the subsequent peritectic conversion of NiAl to $Ni_2Al_3$ but, as the NiAl + L $\rightarrow$ $Ni_2Al_3$ peritectic always appears to go to completion, these two pathways will still result in an initial $Ni_2Al_3$ solid. Further $Ni_2Al_3$ will grow as the local temperature within the particle drops, until such time as this reaches the $Ni_2Al_3$ + L $\rightarrow$ $NiAl_3$ peritectic temperature, wherein the PR and SSPT phase of peritectic solidification will convert some of the $Ni_2Al_3$ to $NiAl_3$. Further cooling will then result in the direct growth of $NiAl_3$ from the liquid. This will continue until the Al-$NiAl_3$ eutectic temperature is reached, wherein the remaining liquid will solidify.

We conjecture that the main source of variability between droplets is the undercooling at which primary solidification is nucleated. This variability will arise due to the melt sub-division effect described in the introduction giving rise to variability in the undercooling at which primary solidification is nucleated. In general terms the effects of increased undercooling will be:

i) a reduction in the scale of the microstructure;
ii) a change in the composition of the primary phase. For the case in which the liquidus and solidus lines are of positive slope (which is the case for the Ni-Al system as plotted in **Figure 1**) the primary phase will become less solute rich as the undercooling increases;
iii) a higher volume fraction of the primary solidification phase, particularly if the undercooling is sufficiently high that any intervening peritectic or eutectic phase transformation can be bypassed;
iv) the formation of metastable phases.

Considerations (i)-(iv) will apply to any metallic melt being subject to gas atomization and we should therefore expect the type of variability observed in this study to be ubiquitous in gas atomized powders, although the extent to how the four considerations listed above impact the final product is, of course, dependent upon the alloy system being considered. Exactly this type of stochastic variation has recently been observed by [31] in a study of Ni-15.0 at% Fe- 25.0 at% Si metal powders. During slow cooling of such powders the normal solidification morphology is a coarse lamellar structure comprising the stable $Ni_{31}Si_{12}$ and $\beta_1$-$Ni_3Si$ phases, although [31] found that in their 212-150 μm diameter sieve fraction approximately 7% of particles solidified to a highly refined lamellar structure with a further 7% solidifying to the metastable single-phase $Ni_{25}Si_9$. In the 150-106 μm diameter sieve fraction, which was the next smallest considered by [31], these fractions increased to 18 and 30% respectively, leading [31] to attribute these differences to the level of undercooling achieved by individual droplets at nucleation, which will increase with increasing cooling rate.

In relation to the Ni-Al system, (iii) is clearly important to the catalytic activity which is known to be strongly dependent upon the phase composition of the catalyst [6] and (i) will also play a role in this respect as a finer scale microstructure would be expected to facilitate the SSPT stage of the peritectic conversion of $Ni_2Al_3$ to $NiAl_3$ due to the higher specific surface area of the $Ni_2Al_3$ dendrites. As discussed above (iv) may be important at very high cooling rates but is not likely to have an impact on the 212-150 μm diameter particles discussed here while (ii) is discussed in detail below.

It is generally assumed that during cooling and solidification, droplets in the < 1 mm size range will be approximately isothermal, although the results presented here and in [21] would seem to contradict this assumption. To assess the viability of sustaining a differential thermal gradient across such small droplets a simple numerical model has been employed. Assuming radial symmetry, the cooling of a spherical droplet during solidification can be described by

$$\rho c_{\mathrm{p}} \frac{\partial T}{\partial t} = \frac{1}{r^2}\frac{\partial}{\partial r}\left(\kappa r^2 \frac{\partial T}{\partial r}\right) + L\frac{\partial f}{\partial t} \qquad (2)$$

where $\rho$ is the density of the droplet material, $c_{\mathrm{p}}$ the specific heat capacity, $\kappa$ the thermal conductivity and $L$ the specific heat capacity. Values for these parameters appropriate to the Al-27.5 at.% Ni alloy studied here are given in Table I. $f$ is the solid fraction, which is given by [32] as

$$f = 1-(1-f_{\mathrm{R}})\left\{\frac{T_{\mathrm{S}}-T_{\mathrm{R}}}{T_{\mathrm{S}}-T}\right\}^{1/1-k_E} \qquad (3)$$

where $f_{\mathrm{R}}$ is the solid fraction at the end of recalescence, $T_{\mathrm{S}}$ is the solidus temperature, $T_{\mathrm{R}}$ the temperature attained at the end of recalescence and $k_{\mathrm{E}}$ the equilibrium partition coefficient.

Table I – Thermophysical properties used in the Al-27.5 at.% Ni cooling model

| Quantity | Value | Range of application | Units |
|---|---|---|---|
| κ | $55.8 + 0.048T - 4.9\times10^{-5}T^2$ | T < 1132 K | W m $K^{-1}$ |
| κ | 55.8 | T > 1132 K | W m $K^{-1}$ |
| $c_p$ (sol) | 701 + 0.183(T-273) | T < 1132 K | J $kg^{-1}$ $K^{-1}$ |
| $c_p$ (liq) | 1200 | T > 1398 K | J $kg^{-1}$ $K^{-1}$ |
| $c_p$ (mush) | $f$* $c_p$ (sol) + (1-$f$)* $c_p$ (liq) | 1132 ≤ T ≤ 1398 K | J $kg^{-1}$ $K^{-1}$ |
| $L$ | 43630 | | J $kg^{-1}$ |
| ρ | 3590 | | Kg $m^{-3}$ |

Equations (2) & (3) are solved using a simple 1-D finite difference scheme, wherein the temperature $T(r, t)$ at arbitrary time $t$ after recalescence can be calculated. From this we calculate the cooling rate, $\dot{R}(r)$, as the local temperature approaches the peritectic temperature and hence estimate the time available near the peritectic temperature, $\tau(r)$. The results of one such calculation are shown in **Figure 11**, where

we plot $\sqrt{\tau(r)}$ against $r$ as, with reference to Equation (1), this will give a measure of the thickness, $\Delta$, of the layer transformed during the SSPT phase of the peritectic transformation. Moreover, for a thin layer, this will also approximate the transformed volume. In order to avoid consideration of the interdiffusion coefficient in the solid-state, which is not known for this system, we have presented the results relative to a characteristic time, $\tau_0$, where $\tau_0$ is chosen so as to give the appropriate conversion rate in the centre of the particle.

The calculation has been performed for a particle of radius $R_0$ = 105 μm and subject to a fixed temperature boundary condition at the particle surface. As this is equivalent to perfect thermal transfer between the droplet and its surroundings this will set an upper limit on the internal thermal gradients that can be sustained within the droplet. The temperature of the boundary is set at 800 K. This is based on [18], in which the cooling rate of gas atomized Al-Cu powders in an atomizer configuration identical to that employed here was studied by analysis of the secondary dendrite arm spacing. For a finite heat transfer coefficient at the droplet surface, the internal temperature profile will be closer to isothermal than predicted by the fixed temperature boundary condition utilised here.

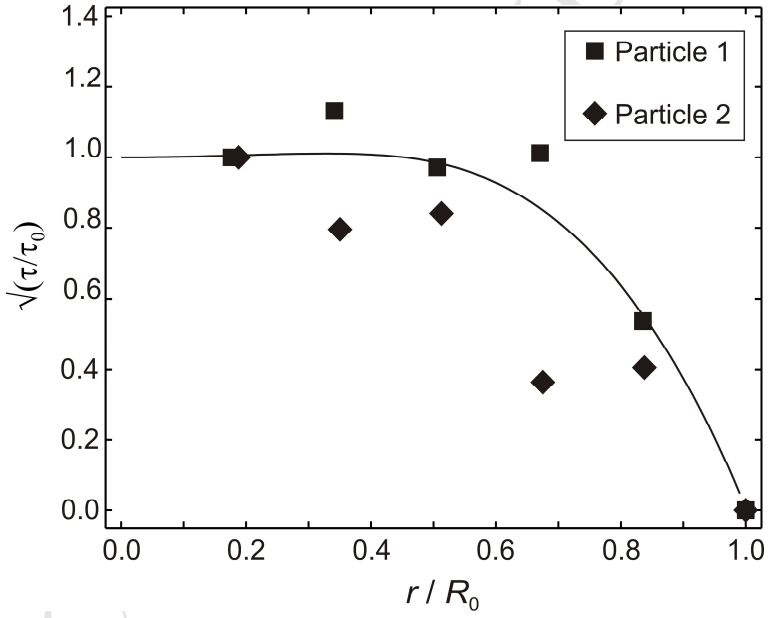


**Figure 11** – Results of the cooling rate calculation (solid line) showing the relative difference in time available for the $Ni_2Al_3$ + L → $NiAl_3$ peritectic transformation as a function of the radial co-ordinate $r$. Also shown the amount of $Ni_2Al_3$ transformed normalised by the peritectic for the two particles shown in **Figure 8** (normalised to 0 at the surface and 1 at the centre of the particle).

As can be seen from **Figure 11**, the model predicts very little transformation of $Ni_2Al_3$ to $NiAl_3$ near the surface of the particle (by virtue of the fixed temperature boundary condition this is by definition zero at $r = R_0$). In contrast, a near constant transformation rate is predicted for $r \leq 0.6R_0$. Also shown in **Figure 11** is an estimate of the amount of $Ni_2Al_3$ that has transformed to $NiAl_3$ for the two particles shown in **Figure 8.** Here we have assumed that there is no transformation at the surface and we have normalised the transformation to 1 at the point nearest the centre of the particle.

As can be seen, the trend is for near constant transformation rate near the centre of the particle with a sharp decline in the volume of $Ni_2Al_3$ transformed near the surface of the particle, approximately matching the predicted trend. This is highly suggestive that the radial variation in phase composition observed here within particles is due to the variation in cooling rate with *r*.

In relation to this we note that $Ni_2Al_3$ is a non-stoichiometric intermetallic and that the actual stability field for $Ni_2Al_3$ spans the composition range 35.9-40.7 at.% Ni. As noted above, notwithstanding any solute trapping effects that might arise during rapid solidification, both the liquidus and solidus lines for the $Ni_2Al_3$ compound have a positive slope, wherein we note that higher undercooling will result in the formation of Ni-lean $Ni_2Al_3$ relative to the notional composition. This will in turn alter the phase composition of the as-solidified product. Conversely, for droplets with zero or very low undercooling the primary solidification phase will be NiAl, with the subsequent rapid peritectic conversion of NiAl to $Ni_2Al_3$. With reference to the Al-Ni phase diagram we note that this should result in the formation of $Ni_2Al_3$ which is Ni-rich relative to the notional composition and to that which forms direct from the melt.

With this in mind we have performed a mass balance calculation to determine the likely composition of the $Ni_2Al_3$ phase on an individual particle basis for each particle analysed. The assumptions used are that the composition of the liquid is uniform and exactly equal to 27.5 at.% Ni, that the $NiAl_3$ phase is exactly stoichiometric (25 at.% Ni) and that the Ni concentration of the Al-eutectic, determined from **Figure 1**, is 2.09 at.% Ni. The range of compositions found is shown in the histogram depicted in **Figure 12**. The particles occupying the region of the distribution that corresponds to the highest Ni content (> 40 at.% Ni) in the $Ni_2Al_3$ phase are also the particles that show the anomalously low $Ni_2Al_3$ phase fraction in **Figure 9a** and the negative difference (more $Ni_2Al_3$ retained in the centre of the particles than at the surface) in **Figure 10**. Once the Ni content of the $Ni_2Al_3$ phase has been fixed it is also possible to use the mass balance calculation to check whether there is any systematic variation in composition across droplets as a function of *r*. This appears not to be the case. In fact, for the particles studied the average difference between the Ni concentration at the surface of the particle and at its centre, was 0.16 at.%. This is comparable to the error that would arise from the quoted $\pm 0.5$ at.% reproducibility in the $Ni_2Al_3$ determination and compares with a 0.18 at.% average difference in bulk composition between particles estimated in the same manner. From this we conclude that there is no significant evidence for a variation in the droplet composition with radial distance.

Although based on relatively small numbers of observations the inference would appear to be that if the $Ni_2Al_3$ is formed via the NiAl + L $\rightarrow$ $Ni_2Al_3$ peritectic, the $Ni_2Al_3$ within the droplet is Ni-rich and is relatively resistant to conversion to $NiAl_3$ via the subsequent $Ni_2Al_3$ + L $\rightarrow$ $NiAl_3$ peritectic. Conversely, $Ni_2Al_3$ formed directly from the melt appears Ni-lean (relative to the notional composition) and more readily able to convert to $NiAl_3$. This would be consistent with Equ. (1) as an Ni-lean composition for the $Ni_2Al_3$ compound would reduce the size of the term $\left(C_\beta - C_\alpha^\beta\right)$ in the denominator, thereby increasing the transformation rate, while conversely an Ni-rich composition will increase the size of the term thereby reducing the transformation rate.

In terms of the crystallography of the $Ni_2Al_3$ phase it is essentially a trigonal extension of the cubic B2 (NiAl) phase with every third plane of Ni atoms perpendicular to the trigonal axis missing [33]. To the Ni-rich side of the stoichiometric composition at 40 at.% Ni, the vacancies associated with the missing plane are progressively filled by Ni atoms but to the Al-rich side of the stoichiometric composition Al replaces Ni on the existing occupied Ni sites [33]. Consequently, an Ni-rich $Ni_2Al_3$ phase may have a lower vacancy concentration than either a stoichiometric or Ni-lean composition, potentially affecting both the nucleation of the $NiAl_3$ phase and the subsequent leaching behaviour of the catalyst.

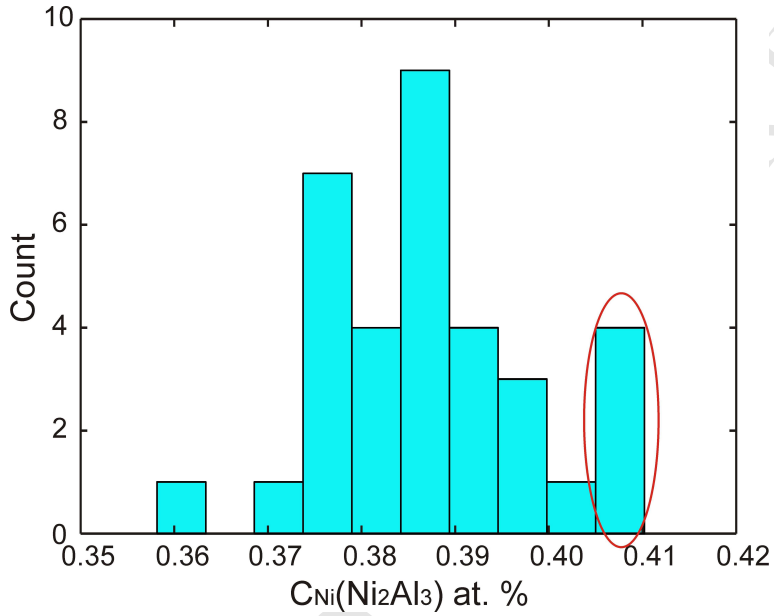


**Figure 12** – Ni content of the $Ni_2Al_3$ phase based on a particle by particle mass balance calculation for the data shown in **Figure 9**. The Ni-rich particles circled are the same group as circled in **Figure 9a**.

The findings presented here allow us to explain a number of aspects of the behaviour of skeletal nickel catalysts produced by gas atomization and have significant implications for the future production and uptake of such catalysts. In particular, the variation in phase composition within particles, and the deficiency of the more catalytically active $NiAl_3$ phase at the particle surface, may explain why post-solidification crushing of the precursor alloy particles enhances the final activity of the catalyst. It would suggest that such crushing is an essential ingredient in obtaining a homogeneous catalyst, due to both the variation within, and between, particles, which in turn may have implications for the financial viability of gas atomized Raney catalysts. Also, the apparent resistance of $Ni_2Al_3$ to undergo the peritectic conversion to $NiAl_3$ at the high cooling rates experienced during gas atomization when the $Ni_2Al_3$ has itself been formed from the peritectic conversion of NiAl, may help to explain why the traditional Raney Ni composition of a 50-50 wt% mixture of Ni and Al performs so poorly when gas atomized. The tendency of $Ni_2Al_3$ formed direct from the melt to participate more readily in the $Ni_2Al_3 + L \rightarrow NiAl_3$ peritectic would then contribute to an explanation as to why Al-rich compositions, which avoid the formation of NiAl, perform so much better in the gas atomized catalyst. On a more general note, gas atomized metal powders are generally assumed to be highly

homogeneous due to the high cooling rates experienced and the lack of segregation, this work indicates that, at least with some alloys, this assumption may not be correct.

## 5 Summary and Conclusions

The main conclusions from this work may be summarised as follows:

- Image analysis has been used to quantify the phase composition of gas atomized Al-27.5 at.% Ni Raney type Ni precursors from backscatter electron images. By dividing each particle into a number of concentric annuli it is possible to quantify both variations within particles (as a function of *r*) and the average variation between particles.
- Within the 150-212 μm size range considered in this study considerable natural variability in phase composition between particles is observed, with the mean and 2 sigma limits for $Ni_2Al_3$, $NiAl_3$ and Al-eutectic being 38.1 ± 5.5, 45.9 ± 6.2 and 16.1 ± 3.3 volume % respectively. This is probably a consequence of variations in the nucleation temperature resulting from the stochastic nature of the nucleation process in small droplets.
- Notwithstanding the variation between droplets, considerable variation in the phase composition was also observed within droplets, with typically more $Ni_2Al_3$ and less $NiAl_3$ being observed at the surface of the particles than in the centre. The average (RMS) excess of $Ni_2Al_3$ at the surface was found to be 2.8 (4.8) vol. %. This appears to be consistent with more rapid cooling at the surface giving less time for the SSPT stage of the $Ni_2Al_3 + L \rightarrow NiAl_3$ peritectic.
- There is some evidence for a relationship connecting the variation between and within droplets. Specifically, droplets which show the lowest overall amount of the $Ni_2Al_3$ phase also tend to show a low difference between the amount of $Ni_2Al_3$ found at surface and centre of the particle (or in some cases less $Ni_2Al_3$ at the surface). This may be related to the origin of the $Ni_2Al_3$ phase and whether it formed direct from the liquid or via the $NiAl + L \rightarrow Ni_2Al_3$ peritectic.

## 6 References

[1] S.R. Montgomery, Catalysis of Organic Reactions, Marcel Dekker, New York, 1981.
[2] Catalytic hydrogenation of carboxylic acids and esters, in, Kyowa Hakko Kogyo Co. Ltd., GB, 1966.
[3] R.J. Allain, V.L. Seale, Acrylonitrile hydrolysis and catalyst useful therefor, in, Nalco Chemical Co., US, 1975.
[4] M. Raney, Method of producing finely-divided nickel, in, US, 1927.
[5] P. Fouilloux, G.A. Martin, A.J. Renouprez, B. Moraweck, B. Imelik, M. Prettre, Texture and structure of Raney nickel, J. Catal., 25 (1972) 212-222.
[6] F. Devred, A.H. Gieske, N. Adkins, U. Dahlborg, C.M. Bao, M. Calvo-Dahlborg, J.W. Bakker, B.E. Nieuwenhuys, Influence of phase composition and particle size of atomised Ni-Al alloy samples on the catalytic performance of Raney-type nickel catalysts, Appl. Catal. A, 356 (2009) 154-161.

[7] A.B. Fasman, V.F. Timofeeva, V.N. Rechkin, Y.F. Klyuchnikov, I.A. Sapukov, Effect of the composition of a nickel-aluminum alloy on the structure and specific activity of a Raney nickel catalyst, Kinet. Katal., 13 (1972) 1513-1519.
[8] R. Wang, H. Chen, Z. Lu, S. Qiu, T. Ko, Structural transitions during aluminum leaching of NiAl3 phase in a Raney Ni-Al alloy, J. Mater. Sci., 43 (2008) 5712-5719.
[9] A.J. Smith, D.L. Trimm, The preparation of skeletal catalysts, Annu. Rev. Mater. Res., 35 (2005) 127-147.
[10] M.L. Bakker, D.J. Young, M.S. Wainwright, Selective leaching of nickel-aluminum ($NiAl_3$ and $Ni_2Al_3$) intermetallics to form Raney nickels, J. Mater. Sci., 23 (1988) 3921-3926.
[11] H. Warlimont, U. Kuehn, N. Mattern, Rapidly quenched Raney catalyst precursors, Mater. Sci. Eng. A, 226-228 (1997) 900-904.
[12] H. Lei, Z. Song, D. Tan, X. Bao, X. Mu, B. Zong, E. Min, Preparation of novel Raney-Ni catalysts and characterization by XRD, SEM and XPS, Appl. Catal. A, 214 (2001) 69-76.
[13] D. Tourret, G. Reinhart, C.-A. Gandin, G.N. Iles, U. Dahlborg, M. Calvo-Dahlborg, C.M. Bao, Gas atomization of Al-Ni powders: Solidification modeling and neutron diffraction analysis, Acta Mater., 59 (2011) 6658-6669.
[14] F. Devred, G. Reinhart, G.N. Iles, B. van der Klugt, N.J. Adkins, J.W. Bakker, B.E. Nieuwenhuys, Synchrotron X-ray microtomography of Raney-type nickel catalysts prepared by gas atomisation: Effect of microstructure on catalytic performance, Catal. Today, 163 (2011) 13-19.
[15] A. Ilbagi, H. Henein, A.B. Phillion, Phase quantification of impulse atomized Al68.5Ni31.5 alloy, J. Mater. Sci., 46 (2011) 6235-6242.
[16] M. Kearns, Development and applications of ultrafine aluminum powders, Mater. Sci. Eng. A, 375-377 (2004) 120-126.
[17] N. Zeoli, S. Gu, S. Kamnis, Numerical modelling of metal droplet cooling and solidification, Int. J. Heat Mass Transfer, 51 (2008) 4121-4131.
[18] A.M. Mullis, L. Farrell, R.F. Cochrane, N.J. Adkins, Estimation of cooling rates during close-coupled gas atomization using secondary dendrite arm spacing measurement, Metall. Mater. Trans. B, 44 (2013) 992-999.
[19] H.W. Kerr, W. Kurz, Solidification of peritectic alloys, Int. Mater. Rev., 41 (1996) 129-164.
[20] D.H. St John, L.M. Hogan, A simple prediction of the rate of the peritectic transformation, Acta Metall., 35 (1987) 171-174.
[21] C.M. Bao, U. Dahlborg, N. Adkins, M. Calvo-Dahlborg, Structural characterisation of Al-Ni powders produced by gas atomisation, J. Alloys Compd., 481 (2009) 199-206.
[22] C. Pohla, P.L. Ryder, Crystalline and quasicrystalline phases in rapidly solidified AI-Ni alloys, Acta Mater., 45 (1997) 2155-2166.
[23] O. Shuleshova, D. Holland-Moritz, W. Löser, G. Reinhart, G.N. Iles, B. Büchner, Metastable formation of decagonal quasicrystals during solidification of undercooled Al-Ni melts: In situ observations by synchrotron radiation, EPL, 80 (2009).
[24] O. Shuleshova, W. Löser, D. Holland-Moritz, D.M. Herlach, J. Eckert, Solidification and melting of high temperature materials: in situ observations by synchrotron radiation, J. Mater. Sci., 47 (2012) 4497-4513.
[25] F. Devred, G. Reinhart, G.N. Iles, U. Dahlborg, M. Calvo-Dahlborg, ESRF Experimental report HS-3612, in, 2009.
[26] V. Anand, A.J. Kaufman, N.J. Grant, Rapid solidification processing: Principles and technologies II, Claitor, Baton Rouge, LA, 1978.

[27] I.E. Anderson, R.S. Figliola, H. Morton, Flow mechanisms in high-pressure gas atomization, Mater. Sci. Eng. A, 148 (1991) 101-114.
[28] M. Libera, G.B. Olson, S. Vander, Heterogeneous nucleation of solidification in atomized liquid metal droplets, Mater. Sci. Eng. A, 132 (1991) 107-118.
[29] A. Ilbagi, H. Henein, J. Chen, D.M. Herlach, R. Lengsdorf, C.-A. Gandin, D. Tourret, A. Garcia-Escorial, Containerless Solidification and Characterization of Industrial Alloys (NEQUISOL), Journal of Physics: Conference Series, 327 (2011).
[30] C.A. Schneider, W.S. Rasband, K.W. Eliceiri, NIH Image to ImageJ: 25 years of image analysis, Nature Methods, 9 (2012) 671-675.
[31] L. Cao, A.M. Mullis, R.F. Cochrane, Solidification morphology and phase selection in drop-tube processed Ni-Fe-Si intermetallics, Intermetallics, 60 (2015) 33-44.
[32] M.C. Flemings, Solidification Processing, McGraw Hill, NY, 1974.
[33] A. Taylor, N.J. Doyle, Further studies on the nickel-aluminium system. I. The beta-NiAI and delta-Ni2AI3 phase fields, J. Appl. Crystallogr., 5 (1972).

- The phase composition of powder Raney-Ni catalysts has been investigated.
- Image analysis is used to quantify differences between and within particles.
- Phase composition can vary by up to 10% between the particle surface and centre.
- Differences of up to 10% in the mean composition are also found between particles.